JTTEE5 19:262–274
DOI: 10.1007/s11666-009-9417-z
1059-9630/$19.00 © ASM International

Peer Reviewed

Microstructures and Functional Properties of Suspension-Sprayed Al_2O_3 and TiO_2 Coatings: An Overview

Filofteia-Laura Toma, Lutz-Michael Berger, Carl Christoph Stahr, Tobias Naumann, and Stefan Langner

(Submitted April 28, 2009; in revised form August 11, 2009)

This paper presents an overview of current research activities regarding the properties and functionalities of finely structured alumina (Al_2O_3) and titania (TiO_2) coatings prepared by suspension plasma spraying and suspension HVOF spraying. A selection of new experimental results obtained by the authors is also included. In the case of Al_2O_3, focus was on the retention of a higher content of the α-phase in the coatings without any post-treatment or alloying. For TiO_2, the goal was to preserve the initial anatase phase in order to obtain photocatalytically active titania coatings. Coating microstructures, phase compositions, and functionalities resulting from the interactions between different working parameters are discussed.

Keywords Al_2O_3, coating, crystalline phase, microstructure, photocatalytic properties, suspension thermal spraying, TiO_2

1. Introduction

Thermal spray processes represent an important group of surface modification and engineering technologies. Besides metals and hardmetals, oxides (Al_2O_3, TiO_2, Cr_2O_3, etc.) are among the most important materials for the preparation of thermally sprayed coatings. Atmospheric plasma spraying (APS) has traditionally been the most commonly used spray process for the preparation of these coatings. High-velocity oxy-fuel (HVOF) spraying allows coatings with reduced porosity, higher bond strength, and lower roughness to be produced (Ref 1).

This article is an invited paper selected from presentations at the 2009 International Thermal Spray Conference and has been expanded from the original presentation. It is simultaneously published in *Expanding Thermal Spray Performance to New Markets and Applications: Proceedings of the 2009 International Thermal Spray Conference*, Las Vegas, Nevada, USA, May 4-7, 2009, Basil R. Marple, Margaret M. Hyland, Yuk-Chiu Lau, Chang-Jiu Li, Rogerio S. Lima, and Ghislain Montavon, Ed., ASM International, Materials Park, OH, 2009.

Filofteia-Laura Toma, Lutz-Michael Berger, Carl Christoph Stahr, Tobias Naumann, and **Stefan Langner**, Fraunhofer Institute for Material and Beam Technology (Fh-IWS), Winterbergstrasse 28, 01277 Dresden, Germany; and **Carl Christoph Stahr**, W.C. Heraeus GmbH, Thin Film Materials Division, Wilhelm-Rohn-Strasse 25, 63450 Hanau, Germany. Contact e-mail: filofteia-laura.toma@iws.fraunhofer.de.

1.1 Alumina (Al_2O_3)

Al_2O_3 is commonly used for the preparation of wear-resistant and electrically insulating coatings. Sintered alumina consists of the only thermodynamically stable modification of alumina, α-Al_2O_3 (corundum). The typical properties of sintered alumina (high melting point, high electrical resistance up to high temperatures, good mechanical properties, and high chemical stability) are associated with the corundum phase (Ref 1). Regardless of the spray process used for their preparation, the thermally sprayed alumina coatings predominantly consist of metastable phases, e.g., γ- or δ-Al_2O_3. This rather atypical behavior was already described in detail about 40 years ago by McPherson (Ref 2, 3). Thermally sprayed coatings are currently produced with this phase transformation being either ignored or accepted. Despite this transformation, coating properties are still acceptable for many applications. However, significant differences between these phases exist, e.g., regarding long-term stability in humid environments and the resultant effects on the electrical insulating properties. In many cases, there is a great need to obtain coatings consisting of α-Al_2O_3. Different approaches have been proposed for achieving this. One of the solutions was the post-heat treatment of coatings at temperatures above 1200 °C, the temperature at which γ-Al_2O_3 transforms to α-Al_2O_3 (i.e. Ref 4, 5). However, due to the lower density of the γ-structure (3.6 g cm^{-3} compared with about 4.0 g cm^{-3} for α-Al_2O_3), heat treatment results in an increase of microstructural defects, e.g. cracks in the coating. Heating at a temperature of 1350 °C for a prolonged period results in coating densification by sintering; moreover, heat treatment does not represent an acceptable solution for many coated metallic substrates.

Heintze and Uematsu (Ref 6) showed that through use of the same spraying conditions (gases and spray distance)

but a different torch traverse speed, coatings containing >99.5% γ-Al_2O_3 or coatings with high α-Al_2O_3 contents could be prepared. The authors proposed a slow torch speed with little or no air cooling to ensure slower cooling conditions, and, consequently, solidification as a solution for obtaining coatings with high α-Al_2O_3 contents.

Several studies aimed at retaining α-Al_2O_3 proposed the use of special spray processes such as high-frequency plasma spraying (HFPS) or inductive coupled plasma (ICP) or of specific spraying conditions (large substrate torch distances, low currents, and high plasma pressures), as was mentioned in several previous studies, including those by Kreye (Ref 7), Dzur (Ref 8), and Müller and Kreye (Ref 9).

The most promising results regarding stabilization of the α-phase in the sprayed alumina coatings were obtained by alloying with other oxides, mostly Cr_2O_3 (Ref 10-12).

1.2 Titania (TiO_2)

Extensive studies have been conducted on titanium oxide coatings due to their multifunctional character and the diversity of their existing and potential applications. For example, titanium oxide coatings are applied or under investigation for use in electrical, solid-lubrication, mechanical, and biomedical applications (e.g., Ref 13, 14). Several of these applications are closely connected with the ability of titanium dioxide, as the most important oxide in the Ti-O system, to lose oxygen easily and to form titanium suboxides with planar stacking faults (Magnéli phases) (Ref 15).

Following the initial work of Fujishima and Honda (Ref 16) on the photoelectrochemical process for solar energy conversion and water photolysis on TiO_2 electrodes, extensive studies on TiO_2 for photoelectrical and photocatalytic applications have been carried out over the last few decades. Special attention has been paid to TiO_2 for these types of applications due to its availability, relatively low costs, higher chemical stability, and nontoxic properties. Titanium dioxide can be used as a photocatalyst for decomposition and removal of waste organic compounds and harmful gases from water and the atmosphere or for hospital sterilization applications. An extensive review of photocatalysis and TiO_2 as a photocatalyst was published by Fujishima et al. (Ref 17).

For photocatalytic applications, TiO_2 can be used in the form of a powder or a coating deposited by any of numerous techniques (sol-gel, spray pyrolysis, chemical vapor deposition, physical vapor deposition, anodic oxidation, etc.). In recent years, thermal spraying has been gaining in interest as a method for the preparation of titanium oxide coatings with effective photocatalytic performance (Ref 18, 19). Compared with other methods, this technique offers the possibility of producing large active surfaces with a high rate of deposition and high mechanical stability and with promising economic prospects for industrial scale-up.

As a surface process, photocatalysis occurs only in the very thin upper layer of the titania coating, and hence significant attention has to be paid to the morphological and microstructural characteristics of the titania coatings.

The most important modifications of titanium dioxide are rutile and anatase. At higher temperatures, the latter transforms irreversibly into rutile. It is generally assumed that anatase exhibits a higher photocatalytic activity than rutile does. However, the presence of a certain amount of rutile in the coatings has been shown to enhance the photocatalytic performance (Ref 20).

Due to the irreversible phase transformation of anatase to rutile occurring during thermal spraying, efforts have been made to preserve a higher amount of anatase in the coatings. Various solutions have been proposed for stabilizing the anatase. Bertrand et al. (Ref 21) confirmed the presence of a significantly higher anatase phase content (up to 80 vol.%) in the plasma-sprayed TiO_2 coatings prepared in low-energy spraying conditions (plasma power of <10 kW) and starting from a spray-dried titania powder with a large granule size (+90 μm). Nonetheless, no discussions on the photocatalytic activity of such coatings were given. Other authors proposed the stabilization of the anatase phase in the coatings through the addition of dopants such as ion metals or oxides (e.g., Ref 22-25). In order for the photocatalytic performance of the titania coatings to be improved, the concentration of the dopant must not exceed an optimal value; otherwise, the activity will be decreased. More promising results have been obtained for titania coatings prepared by thermal spraying with liquid precursors of pure titania or ion-doped titania.

1.3 Suspension Thermal Spraying

Modified thermal spraying processes using suspensions of fine powders or organic/inorganic solutions as starting materials have been developed since the beginning of the 90s. Compared with conventional thermal spray methods, the suspension spraying technique presents some advantages: the possibility of directly feeding fine nano- and submicron-scale particles, the possibility of preserving a higher amount of the initial crystalline phase (in some cases), and the ability to retain the initial crystallite size. Moreover, the technique allows thick and thin, finely structured coatings to be prepared. Use of the suspensions is known, and patents have been granted or applied for, RF inductive plasma spraying, DC plasma spraying, and HVOF spraying (Ref 26-29). Even though there are some limitations associated with it, suspension thermal spraying has been successfully used to prepare coatings designated for SOFCs, TBCs, field emitters, photocatalytic applications, biomaterials, photovoltaics, as shown in examples of the literature (Ref 30-37).

This paper presents an overview of the properties and functionalities of finely structured alumina (Al_2O_3) and titania (TiO_2) coatings prepared by suspension plasma spraying (SPS) and suspension HVOF spraying (SHVOF). Coating microstructures and phase compositions resulting from interactions between different working parameters are discussed. A selection of new experimental results obtained by the authors is presented. In the case of Al_2O_3, focus was on the retention of a higher content of the

α-phase in the coatings. For TiO_2, the goal was to preserve the initial anatase phase in order to obtain photocatalytically active titania coatings.

2. Experimental Procedures

2.1 Suspensions

Commercially available Al_2O_3 powders (Almatis GmbH, Ludwigshafen, Germany) were used to prepare aqueous and alcoholic suspensions: A-16 SG, A1000 SGD, and CT3000 SG. The solids load in the suspensions was 20-25 wt.%. In the case of alcoholic suspensions, an organic dispersing agent (from Zschimmer & Schwarz, Lahnstein, Germany) was added to improve particle dispersion and deflocculation. The suspensions were magnetically and ultrasonically stirred to break up the agglomerates and to avoid reagglomeration of the particles.

Stable aqueous titania suspensions were prepared by dispersion of 10 and 20 wt.% of fine Aeroxide TiO_2 P25 nanopowder (Evonik Degussa GmbH, Frankfurt/Main, Germany) in distilled water.

A summary of feedstock powders and suspension formulations is given in Table 1.

2.2 Suspension Spraying Setups

Suspension spraying was adapted to both APS and HVOF spray processes. The feedstock slurries were supplied from a modified pressurized reservoir (Krautzberger GmbH, Eltville/Rhein, Germany), as described in the authors' previous work (Ref 38). The pressure in the vessel was varied (between 0.15 and 0.5 MPa) in order for good introduction of the liquid into the plasma jet or the supersonic flame to be ensured.

Different suspension injection systems were developed. One of these systems consisted in the external injection of the liquid into the plasma or HVOF flame via two modes: (i) mechanical injection mode, in which the liquid is radially injected in the form of a liquid jet into the plasma/flame, and (ii) spray atomization mode, in which the suspension is first atomized with the help of an inert gas (N_2) before entering the plasma/flame (Ref 39). The other system enabled internal injection of the liquid into the combustion chamber of the HVOF gun. This method results in improved heat transfer between the fine particles and the HVOF flame but presents the disadvantage of the possibility of the injector nozzle becoming clogged after long periods of spraying as a consequence of the formation of solid deposits inside the torch (Ref 40).

The spray parameters were chosen in order for Al_2O_3 coatings with high initial α-phase contents to be obtained, whereas the parameters for the TiO_2 coatings were selected with the aim of preserving the photocatalytically active anatase phase. Plasma spraying was performed with an F6 torch (6-mm nozzle, GTV mbH, Luckenbach, Germany) using different Ar/H_2, Ar/He, or Ar/H_2/He plasma gas mixtures at varying arc currents (from 400 to 750 A) and electric power levels (between 25 and 56 kW). HVOF spraying was carried out with a Top Gun torch (8-mm nozzle, GTV mbH) using ethylene as a fuel gas. The normalized oxygen-to-fuel ratio (λ) was varied from 0.75 to 1.25. The spray distances (shorter than in the case of conventional thermal spraying because of the lower inertia of smaller particles) were chosen as a function of the spray system and the material to be deposited. Alumina coatings were prepared at spray distances varying from 50 to 60 mm in the case of SPS and from 110 to 125 mm with SHVOF. For titania coatings, the spray distances were 60-70 mm for SPS and 90 mm for SHVOF. For SHVOF spraying with the internal injection mode, only aqueous suspensions were used. In order for the risk of injector clogging due to the more rapid evaporation of ethanol compared with water to be diminished, no alcohol-based suspensions were sprayed with internal injection by HVOF. More details about the SPS and SHVOF spray parameters can be found elsewhere (Ref 38, 39).

2.3 Characterization Methods

The microstructures of the coatings were mainly examined by optical microscopy and scanning electron microscopy. The phase compositions were investigated by x-ray diffraction using a D8 Advance Bruker AXS diffractometer. Measurements were carried out in the θ-2θ step scan mode using CuKα radiation and a step size of 0.05. The phases were identified using the *Diffrac EVA software*. The volume percentage of the α-Al_2O_3 phase

Table 1 Feedstock powders and suspension formulations

Powder/commercial name	Crystalline phase	Specific surface area (a), m^2/g	Particle size (a), μm			Suspension formulation
			D_{10}	D_{50}	D_{90}	
A-16 SG	α-Al_2O_3	8.9	…	0.4	1.5	25 wt.% of solid, distilled H_2O, acidic pH
A1000 SGD	α-Al_2O_3	7.6	0.20	0.46	1.9	25 wt.% of solid, pure ethanol, basic pH 2 wt.% dispersant/wt. powder
CT3000 SG	α-Al_2O_3	7.5	…	0.8	2.5	20 wt.% of solid, H_2O, acidic pH
Aeroxide P25	~80 vol.% anatase + rutile	50		…		10 and 20 wt.% of solid, H_2O, acidic pH

(a) Product certificate data sheets

and that of the anatase TiO_2 were determined using the following relations (Eq 2, following Ref 18):

$$C_{\alpha}^{Al_2O_3} = \frac{A_{\alpha}(113)}{A_{\alpha}(113) + 0.89 \cdot A_{\gamma}(400)} \cdot 100(\%) \quad \text{(Eq 1)}$$

$$C_{anatase}^{TiO_2} = \frac{8 \cdot A_{anatase}(101)}{8 \cdot A_{anatase}(101) + 13 \cdot A_{rutile}(110)} \cdot 100(\%) \quad \text{(Eq 2)}$$

with A being the integral area of the respective peak.

The Vickers microhardnesses HV0.3 (load of 2.94 N) and HV0.05 (load of 0.49 N) of the SHVOF Al_2O_3 coatings were measured on cross sections using a HP-Mikromat 1-HMV tester (Hegewald & Peschke Meß-und Prüftechnik GmbH, Nossen, Germany) with load duration of about 10 s. The given microhardness was the average value of ten indentations.

The photocatalytic activity of the titania coatings was evaluated based on different methods: degradation of gaseous acetaldehyde, decoloration of pink dye Rhodamine B (RB), and decoloration of an aqueous solution of methylene blue (MB). The first two photocatalytic tests were detailed in a previous work (Ref 39). The degradation of gaseous acetaldehyde was investigated in a hermetically sealed test box specifically developed by ArcelorMittal Liège R&D (Belgium) for measurement of the photocatalytic activity of TiO_2 for air purification. The decoloration of RB was performed at the laboratory LABEIN-Tecnalia/CSIC (Derio, Spain). The test involved the colorimetric degradation of the impregnated dye on the coating under UV irradiation.

Degradation of an aqueous solution of MB was investigated at Fraunhofer IWS following the German standard DIN 52980 (Ref 41). The TiO_2 sample (2.5×2.5 mm^2) was immersed in a 10-µM aqueous solution of MB; after the adsorption equilibrium between MB and TiO_2 was reached, the system was irradiated for 3 h with a UV lamp ($\lambda = 366$ nm). The absorbance of MB before and after the photocatalytic test was measured by UV-VIS spectroscopy (using a Varian Cary 5000 spectrometer, Varian Deutschland GmbH, Darmstadt, Germany) at $\lambda = 664$ nm.

3. Results and Discussion

3.1 Suspension-Sprayed Alumina Coatings

3.1.1 Microstructures of Coatings. The microstructures of the coatings were sensitive to the spraying technique used as well as to the nature of the suspensions.

In the case of suspension plasma spraying, different coating microstructures from dense to porous can be prepared through variation of the operating parameters, such as plasma gases, spray distances, suspension properties, etc. (Ref 42). Selected microstructures resulting from suspension plasma spraying are presented in Fig. 1 for illustrative purposes. Well-melted particles that traveled into the hot zones of the plasma alternated with nano- or submicrometer-sized spherical particles. These spherical

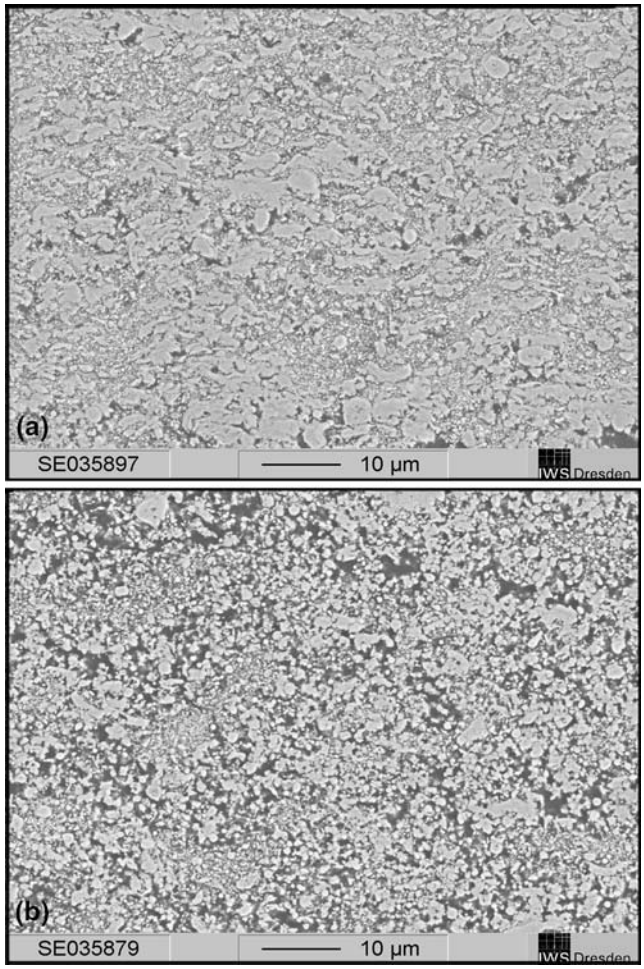

Fig. 1 SEM micrographs of SPS Al_2O_3 A-16SG coatings obtained by injection of an (a) aqueous suspension, plasma conditions: 40Ar-10H_2-55 kW, and (b) alcoholic suspension, plasma conditions: 40Ar-25He-51 kW. Detailed operating parameters can be found elsewhere (Ref 38)

particles resulted from those that traveled into the outer zones of the plasma (particles deviated from the core to the fringes of the plasma due to the thermophoresis force) or from those that already solidified before impact on the substrate due to their low thermal inertia (Ref 43).

Spraying into Ar-H_2 plasma gases resulted in more porous coatings compared with that prepared by injection of the suspension into Ar-He or Ar-H_2-He plasma gas mixtures. The dependence of the microstructure on the operational parameters was largely described by Fauchais et al. (Ref 44). The authors explained and confirmed this by the fact that the phenomena of penetration and fragmentation of liquid drops in the plasma are sensitive to arc instabilities in the DC plasma torch (especially for Ar-H_2 plasma), producing voltage fluctuations and resulting in a plasma jet that varies continuously (in length, position, and velocity). As a consequence, each liquid drop or particle has its own spatial and temporal history when it passes through the plasma. Thus, depending on the

voltage fluctuations, the liquid penetrates either at the edge or close to the jet axis. Reduced drop penetration resulted in particles impacting the substrate in a partially melted state, which in turn led to porosity in the coating microstructure. With the use of helium, the arc fluctuations were lower and the droplets penetrated more uniformly into the core of the plasma jet. Formation of porous coatings can be also explained by low impact velocities of smaller particles and a low Stokes number (Stokes number has to be larger than 1 for the particles to impact the substrate) (Ref 44, 45).

Our results showed that the plasma spraying of an alcoholic suspension resulted in more porous coatings than those prepared from an aqueous suspension, even when an Ar-He plasma gas mixture was used (see Fig. 1b). This observation could be explained by the relatively ''high'' spray distance of about 50 mm. Tingaud et al. (Ref 46) showed that dense and cohesive alumina SPS coatings were obtained when a 10 wt.% Al_2O_3 alcoholic suspension was sprayed at 30 mm, whereas a porous and poorly cohesive coating resulted from a suspension containing 20 wt.% solid charge and a spray distance of about 50 mm.

In contrast to SPS coatings, thick and dense alumina coatings have been prepared by the SHVOF technique using the internal injection of the aqueous suspensions into the combustion chamber of a modified HVOF torch (Ref 47). This is due to better heat transfer (longer dwell time of particles in the enthalpic flame) and better momentum transfer from the HVOF flame to the droplets/particles. An example of the microstructure of such coatings is given in Fig. 2. Depending on the spray parameters and suspension properties, the average coating thickness deposited per pass varied from 2 to 10 μm, comparable to that obtained for SPS coatings (from 4 to 8 μm per pass). In high-magnification SEM micrographs, the SHVOF coatings showed a specific microstructure of melted and partially melted particles, as well as agglomerated fine spherical particles anchored in the structures of the melted particles (Fig. 3). With an increase in the total gas flow

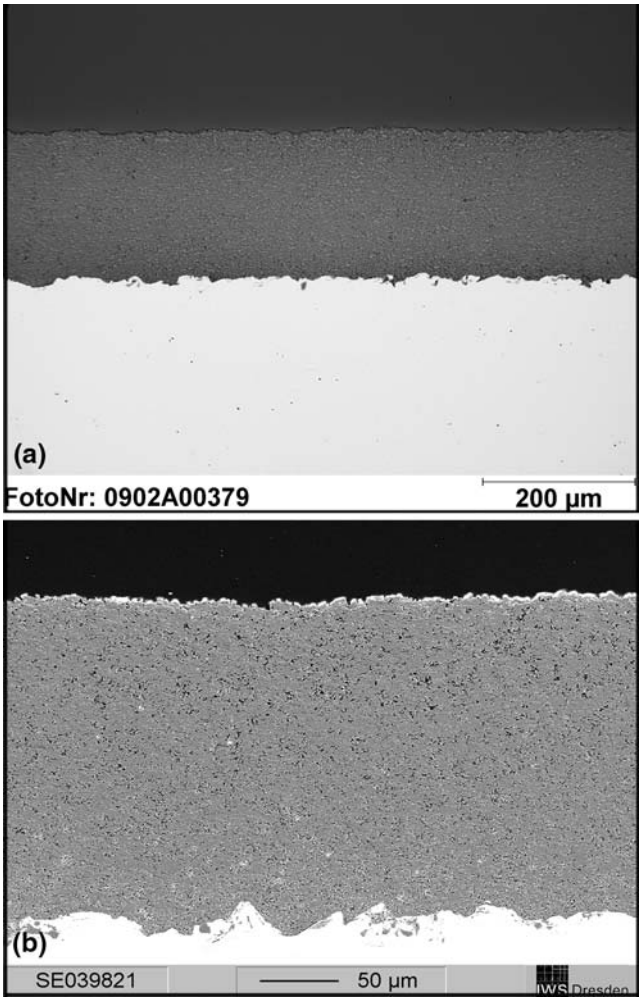

Fig. 2 Microstructures of SHVOF Al_2O_3 coatings starting from aqueous suspension of CT3000SG powder: (a) optical micrograph and (b) SEM image. Spray parameters: $75C_2H_4/230O_2$, λ: 1.0

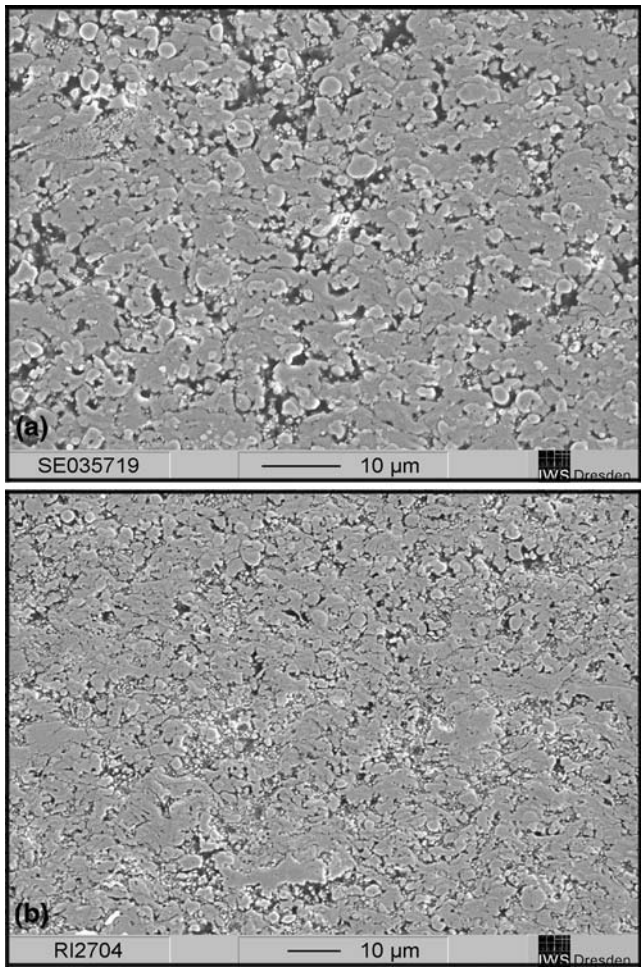

Fig. 3 SEM micrographs of SHVOF coatings starting from aqueous alumina suspensions of (a) A-16 SG powder and (b) A1000 SGD powder. HVOF spray parameters: $60C_2H_4/165O_2$, λ: 0.9

rates, the content of the agglomerated, tiny spherical particles in the coatings decreased, whereas that of melted particles increased, as illustrated in the micrographs given in Fig. 4.

The simulation results of the phenomena occurring during the SHVOF process showed that the evaporation of the liquid involves a cooling effect, which has an influence on the enthalpic energy of the flame (Ref 48). With an increase in the total gas flow rates (and, in the same way, an increase in the energy and velocity of the flame), the evaporation of the liquid solvent will have a lesser cooling effect on the flame; consequently, more heat and momentum will be transferred to the particles, which will remain molten until impact on the substrate. Splat collections on cold, mirror-polished stainless steel substrates as well as the top-view SEM micrographs presented in Fig. 5 confirmed these assumptions. The top views of the coatings illustrated in Fig. 5(b) and (d) showed different types of particles: flattened lamella of more or less regular shape, microsized spherical particles, and nanosized spherical particles. These differences in particle morphologies could be also due to the relatively broad particle size distribution in the powder/suspension, as well as due to the HVOF flame fluctuations during spraying (Ref 48). After impact, the molten particles formed lamellae with sizes of 1-5 μm or even more, which were higher than that of the particles in the initial powder or suspension. Similar results were also obtained by Bolelli et al. (Ref 40) and, in the case of suspension plasma spraying, by Fauchais et al. (44).

3.1.2 Crystalline Phase Compositions of Suspension-Sprayed Al_2O_3 Coatings. X-ray diffraction analysis was used to evaluate the crystalline phase compositions of the suspension sprayed coatings. The XRD patterns of selected suspension-sprayed Al_2O_3 coatings are given in Fig. 6. The crystalline phases were identified using the JCPDS standard cards 46-1212 (corundum) and 10-0425 (γ-Al_2O_3). The significant content of the stable α structure in relation to the content of the metastable γ-phase was noteworthy. Traces of amorphous phases were also

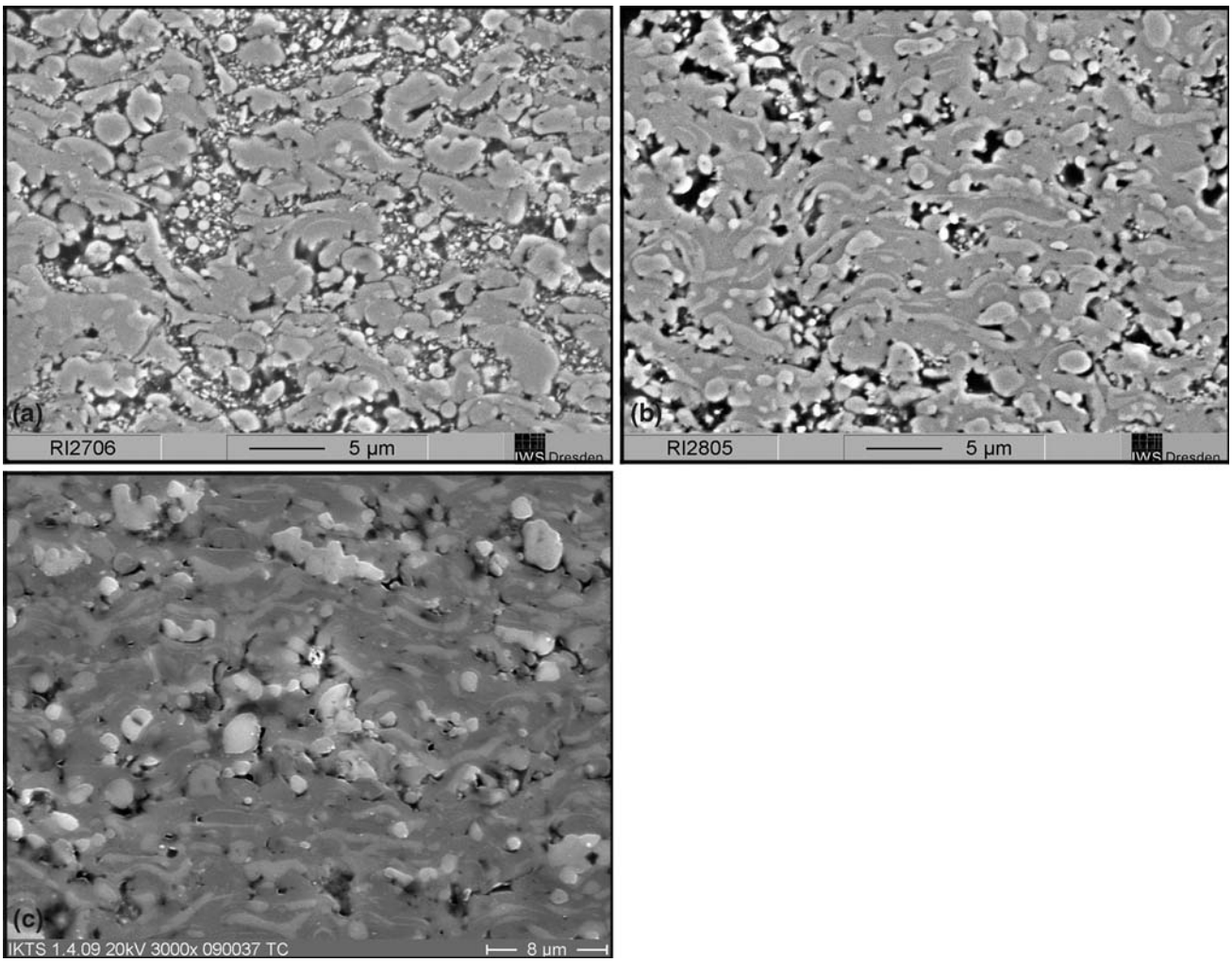

Fig. 4 High-magnification SEM micrographs of SHVOF coatings starting from aqueous A1000 SGD suspension sprayed with different spray parameters: (a) $60C_2H_4/165O_2$, (b) $75C_2H_4/203O_2$, and (c) $90C_2H_4/245O_2$, λ: 0.9

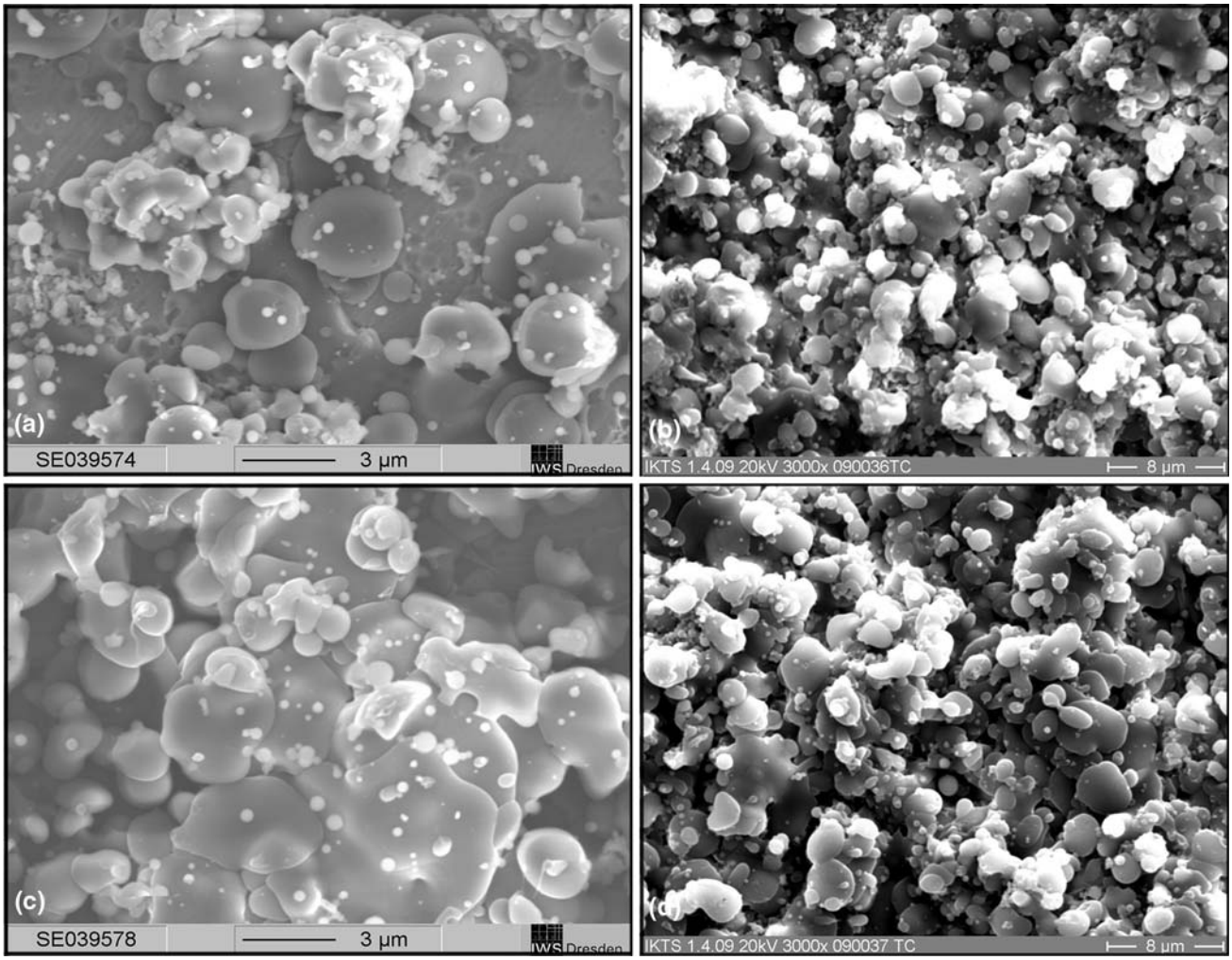

Fig. 5 High-magnification SEM micrographs of splats and top views of SHVOF A1000 SGD coatings obtained with different flame conditions: (1) $75C_2H_4/230O_2$: (a) splats, (b) coating top view; (2) $90C_2H_4/245O_2$: (c) splats, and (d) coating top view

observed in the diffraction patterns. The content of the α-phase in the SPS-sprayed coatings was estimated to be 65-77 vol.%. In the case of SHVOF coatings, a wide range of mean α-to-γ ratios (from about 19 vol.% to about 73 vol.%) was determined (Table 2).

Regarding the coating phase compositions, several authors published results indicating that their suspension-sprayed Al_2O_3 coatings consisted mainly of the metastable γ-phase (see Ref 28, 40, 49). The differences between our results and those found in the literature could be attributed to different grain sizes of the alumina and suspension formulations, as well as the use of different suspension spray systems and spray parameters. Tarasi et al. (Ref 50) showed that through use of the SPS process, coatings with a predominantly α-Al_2O_3 structure or coatings containing mainly of γ-Al_2O_3 could be obtained through variation of the plasma gas composition and the particle size in the suspension.

For conventional thermally sprayed alumina coatings prepared from feedstock powders, the high γ-phase content has been explained by undercooling of the liquid droplets, leading to preferential nucleation of the γ-phase and high cooling rates after solidification of the splats (Ref 2, 51). α-Al_2O_3 is formed in deposits only by nucleation from unmelted seeds, whereas the γ-phase is the result of the solidification of droplets that do not contain these nuclei. According to McPherson (Ref 3), transformation of the initially formed γ-phase to α-Al_2O_3 appears to be possible only if the lamellae formed on impact are thicker than about 10 µm when the substrate is heated to about 1000 °C or if the thickness is greater than about 20 µm on an unheated substrate. The influence of the substrate temperature and, consequently, the cooling rate on the phase composition was demonstrated by Chen et al. (Ref 52). They confirmed that in the case of plasma spraying with substrate temperatures of less than 300 °C, the coating contained γ-Al_2O_3 as the major phase; at a higher substrate temperature (>500 °C), δ-Al_2O_3 was found in the coating due to the transformation of γ- to δ-Al_2O_3 after cooling of the coating. In the case of RF plasma spraying, the coating consisted of α- (as the predominant phase) and δ-Al_2O_3 (Ref 52).

Sokolova et al. (Ref 53) suggested two sources of α-Al_2O_3 in the coating: unmelted α-Al_2O_3 feedstock particles, the amount of which tended to increase with decreasing input power, and secondary α-Al_2O_3 formed as a result of substrate heating. Heintze and Uematsu (Ref 6) confirmed that during plasma spraying with a low torch speed and no/little air cooling, thick coatings containing α-Al_2O_3 were obtained. The particles were well-melted and contained no seed nuclei remaining from unmelted powder particles. An increase in the temperature of the coating would reduce the degree of undercooling in such a way that the nucleation of α-Al_2O_3 from the melt would be preferential to nucleation of γ-Al_2O_3. However, the authors obtained these dense coatings for substrate temperatures higher than 1300 °C.

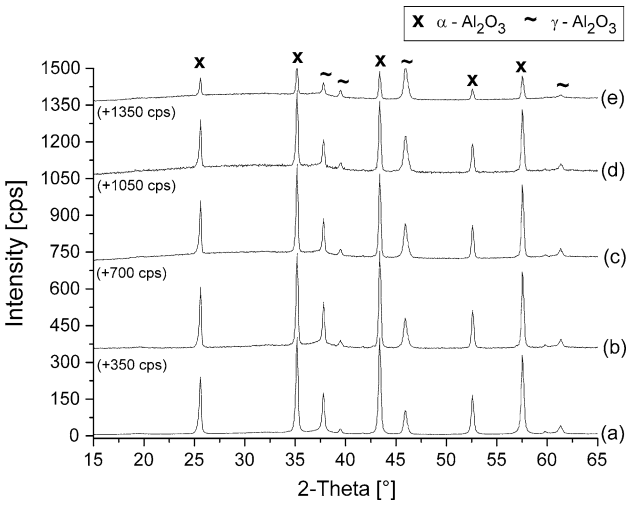

Fig. 6 Diffraction patterns of selected suspension-sprayed Al_2O_3 coatings: (a) SPS A16SG coating from aqueous suspension, plasma conditions: 40Ar-10H_2-55 kW; (b) SPS A16SG coating from alcoholic suspension, plasma conditions: 40Ar-25He-51 kW; (c) SHVOF A1000 SGD coating, flame conditions: 75C_2H_4/203O_2; (d) SHVOF CT3000 SG coating, flame conditions: 75C_2H_4/203O_2 and (e) SHVOF A1000 SGD coating, flame conditions: 90C_2H_4/270O_2

The high content of α-phase in suspension-sprayed coatings does not yet appear to be completely accounted for by the previous explanations. After evaporation of the solvent, the resultant particles were only partially melted or unmelted in the plasma/flame before impacting the substrate—accordingly, the α-phase was mostly preserved in the agglomerated spherical nanoparticles observed in high-magnification SEM micrographs (Fig. 1 and 4a). This is in good agreement with the explanations of McPherson (Ref 2).

Regarding the microstructures of the suspension-HVOF coatings obtained with energetic spraying conditions (see the micrographs of Fig. 4b, c and the coating top views illustrated in Fig. 5b, d), it was confirmed that the content of agglomerated particles decreases significantly with increasing total gas flow rates; thus, the coatings contained structures consisting of lamellar/melted particles, with the α-phase (light gray color) well distributed in the matrix of the γ structure (dark gray in the SEM micrographs due to its lower density compared with that of the α-phase). The presence of melted α-Al_2O_3 in the coating microstructure seems to contradict McPherson's explanation (Ref 2).

It might be possible that the substrate temperatures during spraying (250-400 °C) played a positive role; thus, the cooling of the splat was sufficiently delayed for the particle to recover a grain shape and cool down slowly to obtain α-Al_2O_3. Nonetheless, more systematic studies are required so that a better explanation can be provided for the relatively high content of α-Al_2O_3 in the SHVOF coatings of the present work.

3.1.3 Microhardness Values for SHVOF Al_2O_3 Coatings. The parameters for suspension flame spraying and the nature of the alumina suspensions seemed to affect the mechanical properties of the coatings. The average Vickers microhardness values and the standard deviations are shown in Table 2. When the total gas flow rates were increased and/or when suspensions with larger particle

Table 2 α-Al_2O_3 contents and Vickers microhardness values of selected aqueous suspension HVOF Al_2O_3 coatings as a function of spray parameters

Spray parameters			Average thickness (μm) of coatings from suspensions of:		α-Al_2O_3 content (vol.%) in coatings from suspensions of:		Vickers microhardness of Al_2O_3 coatings from suspensions of:			
							A1000 SGD powder		CT3000 SG powder	
λ	C_2H_4/O_2	Spray distance, mm	A1000 SGD powder	CT3000 SG powder	A1000 SGD powder	CT3000 SG powder	HV0.05	HV0.3	HV0.05	HV0.3
0.75	75/170	110	160	265	72.9	59.1	369 ± 43	309 ± 13	641 ± 127	553 ± 49
	90/203	115	150	…	43.6	…	917 ± 124	737 ± 63	…	…
		125	175	…	50.9	…	637 ± 79	572 ± 45	…	…
0.9	60/165	115	105	…	62.5	…	520 ± 176	…	…	…
	75/203	110	160	230	66.2	59.0	535 ± 58	508 ± 36	790 ± 122	679 ± 29
		115	240	170	57.3	50.8	596 ± 98	545 ± 50	832 ± 130	649 ± 49
	90/245	110	270	215	33.0	19.1	…	796 ± 46	915 ± 118	879 ± 93
1.0	75/230	110	210	190	64.7	59.9	607 ± 62	574 ± 39	722 ± 84	651 ± 43
		115	210	…	62.1	…	765 ± 74	620 ± 52	…	…
	90/270	110	170	240	30.3	50.1	876 ± 78	741 ± 58	912 ± 91	750 ± 86

sizes were used, the SHVOF coating hardness improved from 300 HV0.3 to around 880 HV0.3, with the latter value being comparable to that of a conventional HVOF Al_2O_3 coating (see, e.g., the values in Table 4 in the paper published by Berger et al. 54). In their work, Bolelli et al. (Ref 40) showed that the suspension-sprayed alumina coatings presented slightly higher mechanical properties (microhardness, elastic modulus) than those of conventional HVOF-sprayed coatings.

The slight increase in the hardness values with increasing total gas flow rates or particle size in the powder could be explained by the presence of larger flattened lamellae, which provided larger contact regions between splats and less defective impingement.

3.2 Suspension-Sprayed Titania Coatings

3.2.1 Microstructures of Coatings. As mentioned above, for the titania coatings, the spray parameters were chosen with the aim of retaining a significant amount of the photocatalytically active anatase phase (Ref 38, 39). At the same time, the energies of the plasma and the HVOF flame had to be sufficiently high for obtaining cohesive coatings.

The coatings prepared by mechanical injection of an aqueous suspension into an Ar-H_2 or Ar-H_2-He plasma gas mixture at a low electric power input (26-30 kW) appeared to be dense in the SEM micrographs (Fig. 7a, b) but had structures consisting of finely stacked nanoparticles (Fig. 7c), as already mentioned in a previous work (Ref 34). Although a relatively high thickness deposited per pass was reached (from 4 to 10 μm), the cohesion of the coatings was relatively poor.

External injection of the suspension into the HVOF flame led to coatings presenting superior cohesion to that of the SPS coatings. The SHVOF titania coatings exhibited a bimodal microstructure: regions of partially melted or unmelted particles alternating with zones consisting of well-melted particles (Fig. 8). No significant differences in the microstructures of the SHVOF coatings were observed for the different external modes of suspension injection (spray atomization and mechanical injection modes). Nevertheless, variations were found in coating thickness deposited per pass; it decreased from 4 to 6 μm per pass in

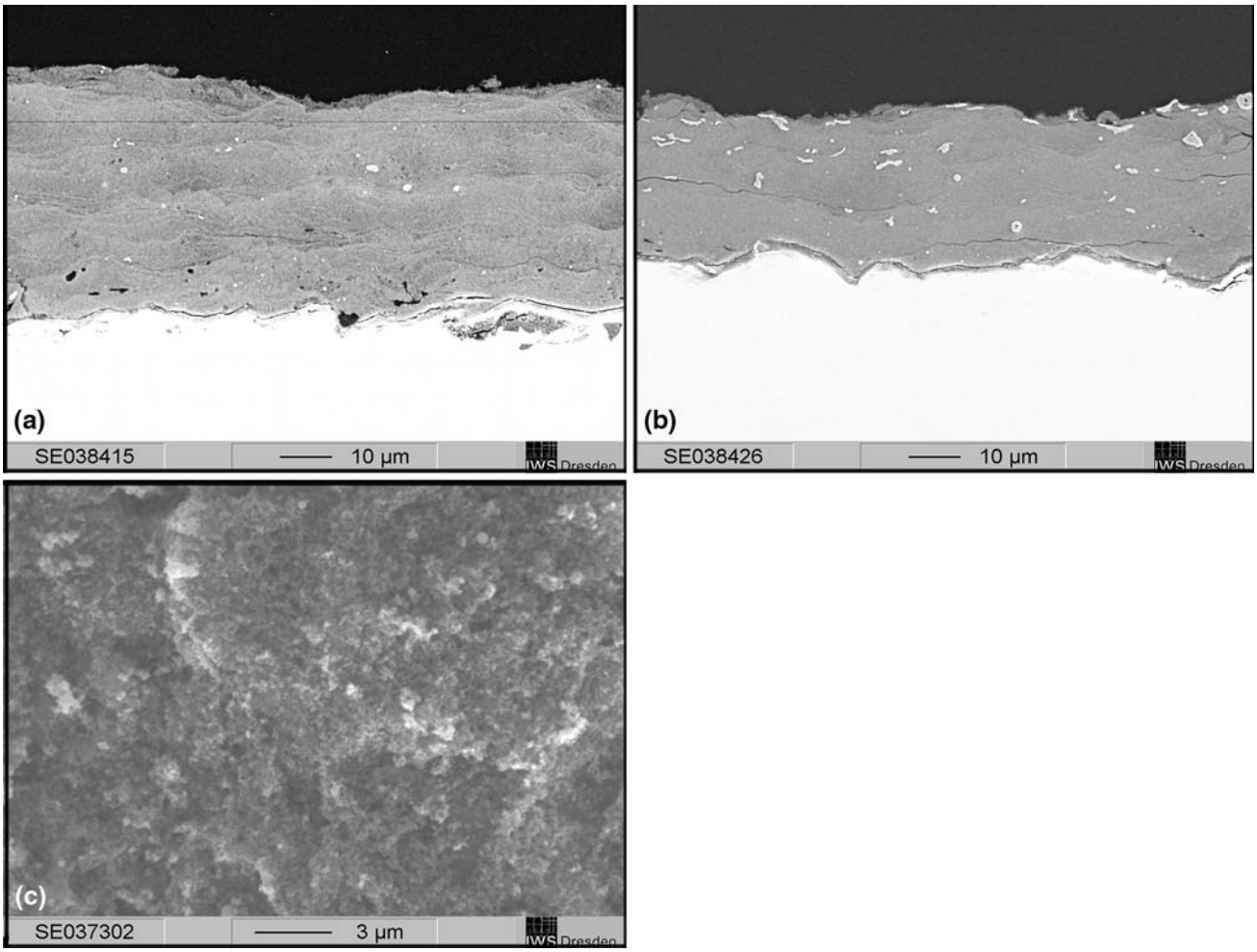

Fig. 7 SEM micrographs of SPS coatings obtained by mechanical injection of 20 wt.% TiO_2 aqueous suspensions into different plasma gas mixtures: (a) 40Ar-3H_2-26 kW; (b, c) 40Ar-3H_2-20He-30 kW [cross section (b) and top view (c)] (Ref 39)

the case of mechanical injection to 1.5 to 2 μm per pass when the suspensions were injected with the spray atomization mode. An increase in the total gas flow rates ensured an improvement in the cohesion and mechanical stability of the SHVOF titania coatings obtained by external injection due to the presence of a higher content of well-melted particles.

By internal injection of a 10 wt.% aqueous suspension into the combustion chamber of the HVOF gun, densely structured coatings with a significantly higher content of melted particles were obtained (Fig. 9). Moreover, the coatings presented superior cohesion properties compared with those obtained by external injection of the suspension into the HVOF flame or the plasma. The thickness deposited per pass was estimated to be 6 to 9 μm.

3.2.2 Crystalline Phases in Suspension-Sprayed Titania Coatings. The phase compositions of the suspension-sprayed titania coatings were identified using the JCPDS standard cards 21-1272 (anatase) and 21-1276 (rutile). The diffraction patterns of selected coatings are given in Fig. 10. The content of anatase in the suspension-sprayed titania coatings was related to the suspension spraying method and the spray parameters. The content of the anatase phase in the SPS-sprayed coatings varied from 68 to 81 vol.%. In the case of SHVOF obtained by internal injection of suspension, the anatase content varied from 29 to 41 vol.%, whereas external injection of the suspension resulted in coatings with anatase contents of 37 to 53 vol.%. A more enthalpic plasma/flame involved an increase of the phase transformation from anatase to rutile.

3.2.3 Photocatalytic Activities of Suspension-Sprayed Titania Coatings. In a previous work (Ref 55), the photocatalytic degradation of the gaseous air pollutants nitrogen oxide (NO_x) and sulfur dioxide (SO_2) in the presence of suspension plasma-sprayed titania coatings was studied. The coatings showed photocatalytic selectivity for these pollutants. The titania coatings presented a much

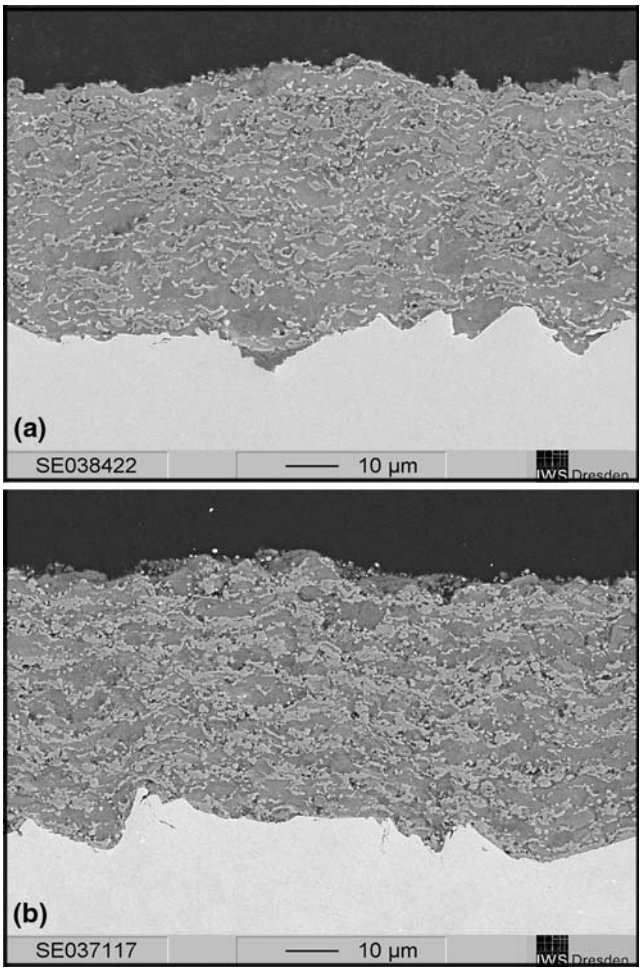

Fig. 8 SEM images of morphologies of SHVOF coatings obtained by external injection of a 20 wt.% TiO_2 aqueous suspension using (a) spray atomization mode and (b) mechanical injection mode. Spraying parameters: $75C_2H_4/203O_2$ (Ref 39)

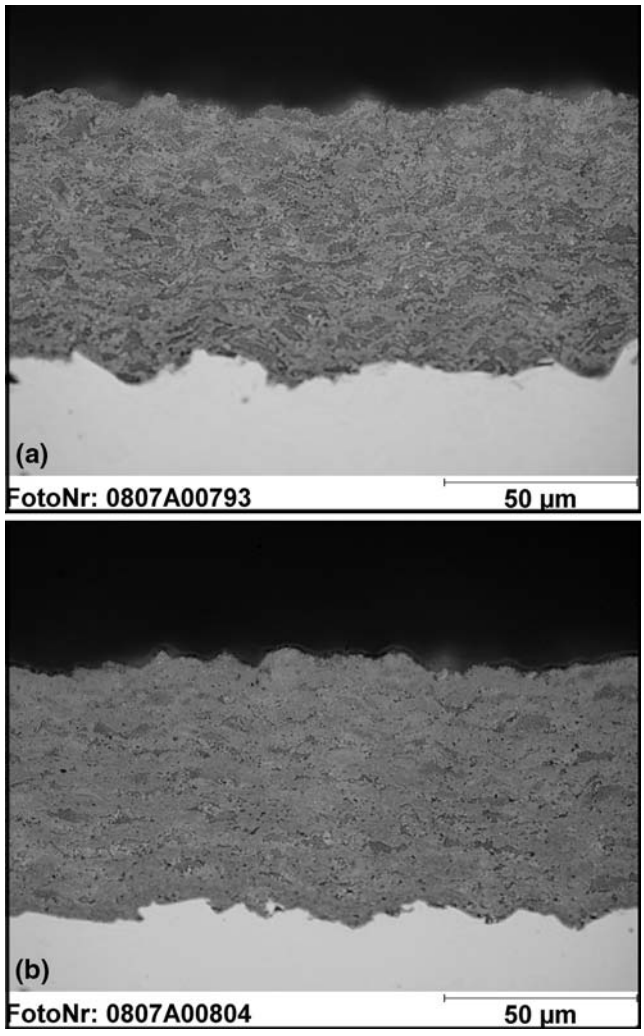

Fig. 9 Optical images of morphologies of SHVOF coatings obtained by internal injection of a 10 wt.% TiO_2 aqueous suspension with different spray parameters: (a) $60C_2H_4/180O_2$, λ: 1.0, and (b) $75C_2H_4/285O_2$, λ: 1.25

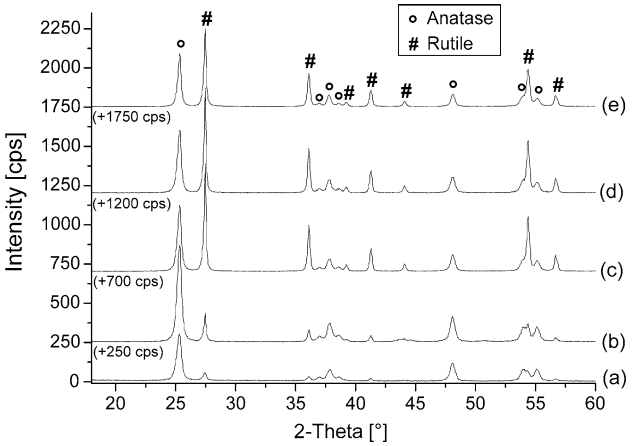

Fig. 10 Diffraction patterns of titania as raw powder and selected suspension-sprayed coatings: (a) P25 raw powder; (b) SPS coating, plasma conditions: 40Ar-3H_2-20He-30 kW; (c) SHVOF coating with external mechanical injection, flame conditions: 75C_2H_4/203O_2; (d) SHVOF coating with external spray atomization mode, flame conditions: 75C_2H_4/203O_2; and (e) SHVOF coating with internal injection mode, flame conditions: 60C_2H_4/180O_2

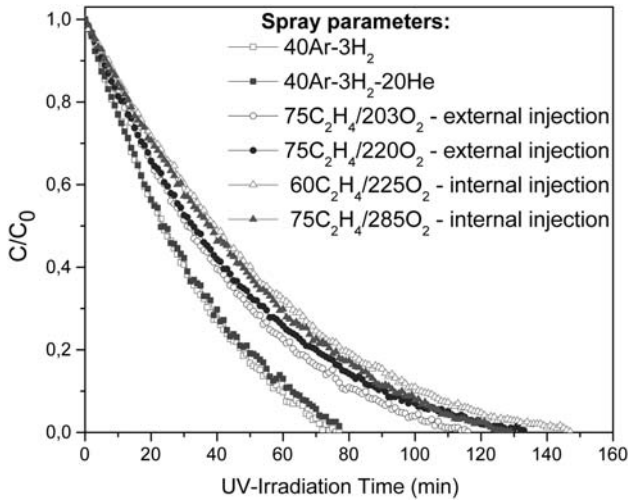

Fig. 11 Photocatalytic removal of acetaldehyde (C/C_0) during UV irradiation in the presence of selected suspension-sprayed titania coatings (Ref 39)

lower activity for degradation of SO_2 than for degradation of nitrogen oxides.

The photocatalytic studies were extended to different organic media: gaseous acetaldehyde, impregnated pink dye Rhodamine B (RB), and aqueous methylene blue (MB) solution. As in the case of inorganic molecules, titania coatings showed different photocatalytic kinetics, depending on the nature of the organic molecule to be degraded. In a previous work published by the authors (Ref 39), it was shown that the complete decolorization of RB was reached after 120 min of UV irradiation in the presence of SPS coatings and after 300 min of UV irradiation in the presence of SHVOF coatings. In the case of gaseous acetaldehyde, the complete degradation was achieved after 80 min of UV light in the presence of SPS coatings and at the latest after 140 min of UV light in the presence of SHVOF coatings (Fig. 11). The photocatalytic degradation of the acetaldehyde followed the kinetics of a pseudo-first order equation, according to the Langmuir-Hinshelwood equation, $\ln\left(\frac{C}{C_0}\right) = -k \cdot t$, with C_0 being the initial concentration of the acetaldehyde at time of irradiation $t_0 = 0$, C being the concentration of pollutant at time t of UV irradiation, and k being the rate constant for degradation of the acetaldehyde (s^{-1}). The values of k were estimated to be 0.0324-0.0350 (s^{-1}) for SPS coatings, 0.0253-0.0257 (s^{-1}) for SHVOF coatings obtained with external injection of the suspension, and 0.0194-0.0216 (s^{-1}) for SHVOF titania coatings obtained by internal injection of the suspension. A higher value of k indicates more rapid degradation of the organic molecule.

In the case of the photocatalytic tests in aqueous media, after 3 h of UV irradiation the extent of degradation of MB was about 30% in the presence of SHVOF coatings obtained by external injection of the suspension and about 20% with SHVOF coatings prepared by internal injection of the suspension.

The different photocatalytic behaviors of titania coatings were mainly correlated with the anatase content. As already reported in the majority of the references, a higher anatase phase content is a determining factor for ensuring faster degradation of the organic pollutants. In our previous work (Ref 39), the dependence of the photocatalytic removal of acetaldehyde on the fraction of anatase phase for selected titanium oxide coatings sprayed from powders and suspensions was shown. A very low removal rate was obtained for the coatings containing less than 15-20 vol.% anatase. The extent of pollutant degradation increased significantly with increasing anatase content (more than 20 vol.%). Moreover, when the anatase ratio exceeded a threshold value (>65 vol.% according to our results), the phase composition contributed less to the degradation of pollutants, and other factors (i.e., physicochemical surface characteristics of titania coatings) became more important (Ref 34).

4. Conclusions

In this article, an overview of current research on the properties and functionalities of alumina and titania prepared by suspension thermal spraying has been given. For both materials, the coatings prepared by APS and HVOF processes using feedstock suspensions were found to differ significantly from those prepared using conventional feedstock powders in terms of their phase compositions and microstructures. Suspension thermal spraying can be used to obtain coatings with economically interesting deposition rates, with the thickness per pass ranging from a few μm to 10 μm or even more.

Through variation of the suspension spraying method and the suspension properties, the microstructure of the

coating can be varied from dense to porous. Densely structured Al_2O_3 coatings with hardness values comparable to that of conventional coatings could be prepared by the suspension HVOF technique. Moreover, it was possible to retain the thermodynamically stable α-Al_2O_3 phase in a wide range (from 19 to 77 vol.%) without posttreatment or alloying. Nevertheless, systematic studies must be performed in order for the high amount of this phase in the suspension-sprayed Al_2O_3 coatings to be explained. The electrical resistivity, the mechanical and tribological properties, and the long-term stability of these coatings will be investigated in further studies.

For photocatalytic applications, special requirements regarding the microstructures and the properties of titania coatings exist. Preservation of the anatase phase, which is decisive for preparation of the photocatalytically active coatings, is one of the main requirements. Moreover, a compromise has to be made between the phase composition, microstructure, and mechanical stability of the coating. The presence of the rutile phase increased the cohesion of the suspension-sprayed titania coatings but decreased their photocatalytic activity. The photocatalytic degradation of different gaseous or aqueous organic media was possible only in presence of thin titania coatings containing more than 15-20 vol.% anatase. However, due to a high rate of deposition and a relatively high mechanical stability, thermally sprayed photocatalytic TiO_2 coatings present an advantage over coatings prepared by other surface modification technologies.

Acknowledgments

The authors thank the following colleagues from Fraunhofer IWS: B. Wolf for metallographic preparation of the samples, A. Richter for SEM analysis, S. Saaro for assistance with XRD analysis, and B. Leupolt for performing of MB photocatalytic experiments. Thanks also go out to G. Michael from Fraunhofer IKTS (Dresden) for the top-view SEM micrographs of alumina coatings. The kind delivery of products from Almatis GmbH is acknowledged. The research on titania was performed within the framework of European Project ''SAPHIR—Safe, integrated & controlled production of high-tech multifunctional materials and their recycling'' (Contract No. 026666-2). The degradation of impregnated Rhodamine B was carried out by I. Villaluenga and Y. de Miguel, Labein-Tecnalia, Derio, Spain. The photocatalytic tests on acetaldehyde have been performed by D. Wicky and D. Jacquet, ArcelorMittal Liege Research, Liege, Belgium. F.-L. Toma wishes to thank the Alexander von Humboldt Foundation (Germany) for her research fellowship (2006-2008) at Fraunhofer IWS, Dresden.

References

1. L.-M. Berger and C.C. Stahr, State and Perspective of Thermally Sprayed Ceramic Coatings in the Al_2O_3-Cr_2O_3-TiO_2 System, *Surface Modification Technologies XXI*, T.S. Sudarshan and M. Jeandin, Ed., 2008, p 469-478
2. R. McPherson, Formation of Metastable Phases in Flame- and Plasma-Prepared Alumina, *J. Mater. Sci.*, 1973, **8**(6), p 851-858
3. R. McPherson, On the Formation of Thermally Sprayed Alumina Coatings, *J. Mater. Sci.*, 1980, **15**(12), p 3141-3149
4. N.N. Ault, Characteristics of Refractory Oxide Coatings Produced by Flame Spraying, *J. Am. Ceram. Soc.*, 1957, **40**(3), p 69-74
5. R.S. Lima and C.P. Bergmann, Phase Transformations on Flame Sprayed Alumina, *Thermal Spray: Practical Solutions for Engineering Problems, Proceedings of 9th National Thermal Spray Conference*, C.C. Berndt, Ed., Oct 7-11, 1996 (Cincinnati), ASM International, 1996, p 765-771
6. G.N. Heintze and S. Uematsu, Preparation and Structures of Plasma-Sprayed γ- and α-Al_2O_3 Coatings, *Surf. Coat. Technol.*, 1992, **50**, p 213-222
7. H. Kreye, Herstellung von Aluminiumoxidschichten mit verbesserten Eigenschaften (Preparation of Alumina Coatings with Improved Properties), University of the Federal Armed Forces Hamburg, Institute for Materials Technologies, Final Report, AiF Founded Project No. 11.466 N, 01.01.1998-31.12.1999 (in German)
8. B. Dzur, Das thermische, induktiv gekoppelte Hochfrequenzplasma: Grundlagen und Möglichkeiten einer außergewöhnlichen Technologie (The Thermal, Inductively Coupled HF-Plasma: Basics and Possibilities of an Extraordinary Technology), *Jahrbuch Oberflächentechnik* 2006, Vol 62, R. Suchentrunk, Ed., Bad Sulgau, Eugen G. Leuze Verlag, 2006, p 131-142 (in German)
9. J.-M. Müller and H. Kreye, Mikrostruktur und Eigenschaften von thermisch gespritzten Aluminiumoxidsschichten (Microstructure and Properties of Thermally Sprayed Alumina Coatings), *Schweissen und Schneiden*, **53**(6), 2001, p 336-345 (in German)
10. P. Chraska, J. Dubsky, K. Neufuss, and J. Pisacka, Alumina-Base Plasma Sprayed Materials Part I: Phase Stability of Alumina and Alumina-Chromia, *J. Therm. Spray Technol.*, 1997, **6**(3), p 320-326
11. J. Ilavsky, C.C. Berndt, H. Herman, P. Chraska, and J. Dubsky, Alumina-Base Plasma-Sprayed Materials—Part II: Phase Transformation in Aluminas, *J. Therm. Spray Technol.*, 1997, **6**(4), p 439-444
12. C.C. Stahr, S. Saaro, L.-M. Berger, J. Dubsky, K. Neufuss, and M. Herrmann, Dependence of the Stabilization of α-Alumina on the Spray Process, *J. Therm. Spray Technol.*, 2007, **16**(5-6), p 822-830
13. L.-M. Berger, Titanium Oxide—New Opportunities for an Established Coating Material, *Thermal Spray Solutions: Advances in Technology and Applications*, on CD-ROM, May 10-12, 2004 (Osaka, Japan), DVS-Verlag GmbH, Düsseldorf, 2004
14. R.S. Lima and B.R. Marple, Thermal Spray Coatings Engineered from Nanostructured Ceramic Agglomerated Powders for Structural, Thermal Barrier and Biomedical Applications: A Review, *J. Therm. Spray Technol.*, 2007, **16**(1), p 40-63
15. P. Waldner and G. Eriksson, Thermodynamic Modelling of the System Titanium-Oxygen, *CALPHAD*, 1999, **23**(2), p 189-218
16. A. Fujishima and K. Honda, Electrochemical Photolysis of Water at Semiconductor Electrode, *Nature*, 1972, **238**, p 37-38
17. A. Fujishima, X. Zhang, and D.A. Tryk, TiO_2 Photocatalysis and Related Surface Phenomena, *Surf. Sci. Rep.*, 2008, **63**, p 515-582
18. A. Ohmori, H. Shoyama, K. Ohashi, K. Moriya, and C. Li, Study of Photo-Catalytic Character of Plasma Sprayed TiO_2 Coating, *Trans. JWRI*, 1999, **28**(1), p 21-26
19. A. Ohmori, H. Shoyama, S. Matsusaka, K. Ohashi, K. Moriya, and C.J. Li, Study of Photo-Catalytic Character of Plasma Sprayed TiO_2 Coatings, *Thermal Spray: Surface Engineer. Via Applied Research*, C.C. Berndt, Ed. (Materials Park, OH), ASM International, 2000, p 317-323
20. G.J. Yang, C.-J. Li, F. Han, and A. Ohmori, Microstructure and Photocatalytic Performance of High Velocity Oxy-Fuel Sprayed TiO_2 Coatings, *Thin Solid Films*, 2004, **466**, p 81-85
21. G. Bertrand, N. Berger-Keller, C. Meunier, and C. Coddet, Evaluation of Metastable Phase and Microhardness on Plasma Sprayed Titania Coatings, *Surf. Coat. Technol.*, 2006, **200**, p 5013-5019
22. F. Ye and A. Ohmori, The Photocatalytic Activity and Photo-Absorption of Plasma Sprayed TiO_2-Fe_3O_4 Binary Oxide Coatings, *Surf. Coat. Technol.*, 2000, **160**, p 62-67

23. Y. Zheng, J. Liu, W. Wu, and C. Ding, Photocatalytic Performance of Plasma Sprayed TiO_2-$ZnFe_2O_4$ Coatings, *Surf. Coat. Technol.*, 2005, **200**, p 2398-2402
24. F.-L. Toma, G. Bertrand, S.O. Chwa, D. Klein, H. Liao, C. Meunier, and C. Coddet, Microstructure and Photocatalytic Properties of Nanostructured TiO_2 and TiO_2-Al Coatings Elaborated by HVOF Spraying for the Nitrogen Oxides Removal, *Mater. Sci. Eng. A*, 2006, **417**, p 56-62
25. Y. Zeng, W. Wu, S. Lee, and J. Gao, Photocatalytic Performance of Plasma Sprayed Pt-Modified TiO_2 Coatings Under Visible Light Irradiation, *Catal. Commun.*, 2007, **8**, p 906-912
26. F. Gitzhofer, E. Bouyer, and M.I. Boulos, Suspension Plasma Spray, U.S. Patent 5,609,921, Filing date: Aug 26, 1994; CA 2198622 C, WO 96/06957 A1; EP 0 777 759 B1
27. K. Valle, P. Belleville, K. Wittmann-Teneze, L. Bianchi, and F. Blein, Nanostructured Coating and Coating Method, Patent FR 0452390, Filing date: Oct 21, 2004; WO 2006/043006 A1; EP 1 802 783 A1; US 2008/0090071 A1
28. J. Oberste-Berghaus, S. Bouaricha, J.-G. Legoux, C. Moreau, and B. Harvey, Method and Apparatus for Fine Particle Liquid Suspension Feed for Thermal Spray System and Coatings Formed Therefrom, Patent Application US 2006/0289405 A1, Filing date: Apr 25, 2006; WO 2006/116844 A1; EP 1 880 034 A1
29. R. Gadow, A. Killinger, M. Kuhn, and D.L. Martinez, Verfahren und Vorrichtung zum thermischen Spritzen von Suspensionen, Patent Application DE 10 2005 0380 453 A1, Filing date: Aug 3, 2005 (in German)
30. E. Bouyer, F. Gitzhofer, and M. Boulos, Parametric Study of Suspension Plasma Sprayed Hydroxyapatite, *Thermal Spray: Practical Solutions for Engineering Problems*, C.C. Berndt, Ed. (Materials Park, OH), ASM International, 1996, p 683-691
31. C. Monterrubio-Badillo, H. Ageorges, T. Chartier, J.F. Coudert, and P. Fauchais, Preparation of $LaMnO_3$ Perovskite Films by Suspension Plasma Spraying for SOFC Cathode, *Surf. Coat. Technol.*, 2006, **200**, p 3743-3759
32. I. Burlacov, J. Jirkowsky, M. Müller, and R.B. Heimann, Induction Plasma-Sprayed Photocatalytically Active Titania Coatings and Their Characterization by Micro-Raman Spectroscopy, *Surf. Coat. Technol.*, 2006, **201**, p 255-264
33. R. Tomaszek, Z. Znamirovski, L. Pawlowski, and A. Wojnakowski, Temperature Behavior of Titania Field Emitters by Suspension Plasma Spraying, *Surf. Coat. Technol.*, 2006, **201**(5), p 2099-2102
34. F.-L. Toma, G. Bertrand, S. Begin, C. Meunier, O. Barres, D. Klein, and C. Coddet, Microstructure and Environmental Functionalities of TiO_2-Supported Photocatalyts Obtained by Suspension Plasma Spraying, *Appl. Catl. B: Environ.*, 2006, **68**(1-2), p 74-84
35. H. Kassner, R. Siegert, D. Hathiramani, R. Vassen, and D. Stoever, Application of Suspension Plasma Spraying (SPS) for Manufacture of Ceramic Coatings, *J. Therm. Spray Technol.*, 2008, **17**(1), p 115-123
36. R. Gadow, A. Killinger, and J. Rauch, New Results in High Velocity Suspension Flame Spraying (HVSFS), *Surf. Coat. Technol.*, 2008, **202**, p 4329-4336
37. R. Vaßen, Z. Yi, H. Kaßner, and D. Stöver, Suspension Plasma Spraying of TiO_2 for the Manufacture of Photovoltaic Cells, *Surf. Coat. Technol.*, 2009, **203**, p 2146-2149
38. F.-L. Toma, L.-M. Berger, T. Naumann, and S. Langner, Microstructures of Nanostructured Ceramic Coatings Obtained by Suspension Thermal Spraying, *Surf. Coat. Technol.*, 2008, **202**(18), p 4343-4348
39. F.-L. Toma, L.-M. Berger, D. Jacquet, D. Wicky, I. Villaluenga, Y.R. de Miguel, and J.S. Lindeløv, Comparative Study on the Photocatalytic Behaviour of Titanium Oxide Thermal Sprayed Coatings from Powders and Suspensions, *Surf. Coat. Technol.*, 2009, **203**(15), p 2150-2156
40. G. Bolelli, J. Rauch, V. Cannillo, A. Killinger, L. Lusvarghi, and R. Gadow, Microstructural and Tribological Investigations of High-Velocity Suspension Flame Sprayed (HVSFS) Al_2O_3 Coatings, *J. Therm. Spray Technol.*, 2009, **18**(1), p 35-49
41. Photocatalytic Activity of Surfaces—Determination of Photocatalytic Activity in Aqueous Medium by Degradation of Methylene Blue, German Standard Draft, E DIN 52980:2007-11 (in German)
42. O. Tingaud, A. Grimaud, A. Denoirjean, G. Montavon, V. Rat, J.-F. Coudert, P. Fauchais, and T. Chartier, Suspension Plasma-Sprayed Alumina Coating Structures: Operating Parameters vs. Coating Architecture, *ITSC 2008: Thermal Spray Crossing Borders*, on CD-ROM, E. Lugscheider, Ed., June 2-4, 2008 (Maastricht, The Netherlands), DVS-Verlag GmbH, Düsseldorf, 2008, p 323-328
43. P. Fauchais, V. Rat, J.-F. Coudert, R. Etchart-Salas, and G. Montavon, Operating Parameters for Suspension and Solution Plasma-Spray Coatings, *Surf. Coat. Technol.*, 2008, **202**(18), p 4309-4317
44. P. Fauchais, R. Etchart-Salas, V. Rat, J.F. Coudert, N. Caron, and K. Wittmann-Ténèze, Parameters Controlling Liquid Plasma Spraying: Solutions, Sols, or Suspensions, *J. Therm. Spray Technol.*, 2008, **17**(1), p 31-59
45. J. Oberste-Berghaus, S. Bouaricha, J.G. Legoux, and C. Moreau, Injection Conditions and In-Flight Particle States in Suspension Plasma Spraying of Alumina and Zirconia Nano-Ceramics, *International Thermal Spray Conference, ITSC 2005*, on CD-ROM, E. Lugscheider, Ed., DVS-Verlag, Basel, Switzerland, 2005
46. O. Tingaud, A. Bacciochini, G. Montavon, A. Denoirjean, and P. Fauchais, Suspension DC Plasma Spraying of Thick Finely-Structured Ceramic Coatings: Process Manufacturing Mechanisms, *Surf. Coat. Technol.*, 2009, **203**(15), p 2157-2161
47. F.-L. Toma, L.-M. Berger, C.C. Stahr, T. Naumann, and S. Langner, Thermisch gespritzte Al_2O_3-Schichten mit einem hohen Korundgehalt ohne eigenschaftsmindernde Zusätze und Verfahren zu ihrer Herstellung, German Patent Application
48. E. Dongmo, A. Killinger, M. Wenzelburger, and R. Gadow, Numerical Approach and Optimization of the Combustion and Gas Dynamics in High Velocity Suspension Flame Spraying (HVSFS), *Surf. Coat. Technol.*, 2009, **203**(15), p 2339-2345
49. J. Rauch, G. Bolelli, A. Killinger, R. Gadow, V. Cannillo, and L. Lusvarghi, Advances in High Velocity Suspension Flame Spraying (HVSFS), *Surf. Coat. Technol.*, 2009, **203**, p 2131-2138
50. F. Tarasi, M. Medraj, A. Dolatabadi, J. Oberste-Berghaus, and C. Moreau, Phase Formation in Alumina/YSZ Nano-Composite Coating Deposited by Suspension Plasma Spray Process, *Thermal Spray 2009: Proceedings of the International Thermal Spray Conference*, B.R. Marple, M.M. Hyland, Y.-C. Lau, C.-J. Li, R.S. Lima, and G. Montavon, Ed., May 4-7, 2009 (Las Vegas, NV), ASM International, 2009, p 409-414
51. A. Vardelle, C. Robert, G.X. Wang, and S. Sampath, Analysis of Nucleation, Phase Selection and Rapid Solidification of an Alumina Splat, *Thermal Spray: A united Forum for Science and Technological Advances*, C.C. Berndt, Ed., Sept 15-18, 1997 (Indianapolis, IN), ASM International, 1997, p 635-643
52. H.C. Chen, E. Pfender, D. Dzur, and G. Nutsch, Microstructural Characterization of Radio Frequency and Direct Current Plasma-Sprayed Al_2O_3 Coatings, *J. Therm. Spray Technol.*, 2000, **9**(2), p 264-273
53. T.V. Sokolova, I.R. Kozlova, Kh. Derko, and A.V. Kiiko, How Certain Physicochemical Properties of Plasma-Deposited Aluminum Oxide Depend on the Deposition Conditions, *Inorg. Mater.*, 1973, **9**(4), p 551-554
54. L.-M. Berger, C.C. Stahr, F.-L. Toma, S. Saaro, M. Herrmann, D. Deska, and G. Michael, Corrosion of Thermally Sprayed Oxide Ceramic Coatings, *Therm. Spray Bull.*, 2009, **2**(1), p 40-56
55. F.-L. Toma, G. Bertrand, D. Klein, C. Coddet, and C. Meunier, Nanostructured Photocatalytic Titania Coatings Formed by Suspension Plasma Spraying, *J. Therm. Spray Technol.*, 2006, **15**(4), p 587-592